

Lab on a Chip

Accepted Manuscript



This is an *Accepted Manuscript*, which has been through the Royal Society of Chemistry peer review process and has been accepted for publication.

Accepted Manuscripts are published online shortly after acceptance, before technical editing, formatting and proof reading. Using this free service, authors can make their results available to the community, in citable form, before we publish the edited article. We will replace this *Accepted Manuscript* with the edited and formatted *Advance Article* as soon as it is available.

You can find more information about *Accepted Manuscripts* in the [Information for Authors](#).

Please note that technical editing may introduce minor changes to the text and/or graphics, which may alter content. The journal's standard [Terms & Conditions](#) and the [Ethical guidelines](#) still apply. In no event shall the Royal Society of Chemistry be held responsible for any errors or omissions in this *Accepted Manuscript* or any consequences arising from the use of any information it contains.

Cite this: DOI: 10.1039/xxxxxxxxxx

Synthetic Microfluidic Paper: high surface and high porosity polymer micropillar arrays[†]

Jonas Hansson,^{a‡} Hiroki Yasuga,^{a‡§} Tommy Haraldsson,^{*a} and Wouter van der Wijngaart^a

Received Date

Accepted Date

DOI: 10.1039/xxxxxxxxxx

www.rsc.org/journalname

We introduce Synthetic Microfluidic Paper, a novel porous material for microfluidic applications that consists of OSTE polymer that is photostructured in a well-controlled geometry of slanted and interlocked micropillars. We demonstrate distinct benefits of Synthetic Microfluidic Paper over other porous microfluidic materials, such as nitrocellulose, traditional paper and straight micropillar arrays: In contrast to straight micropillar arrays, the geometry of Synthetic Microfluidic Paper was miniaturized without suffering capillary collapse during manufacturing and fluidic operation, resulting in six-fold increased internal surface area and three-fold increased porous fraction. Compared to commercial nitrocellulose materials for capillary assays, Synthetic Microfluidic Paper shows a wider range of capillary pumping speed and four times lower device-to-device variation. Compared to the surfaces of the other porous microfluidic materials that are modified by *adsorption*, Synthetic Microfluidic Paper contains free thiol groups and was shown suitable for *covalent* surface chemistry, here demonstrated for increasing the material hydrophilicity. These results illustrate the potential of Synthetic Microfluidic Paper as a porous microfluidic material with improved performance characteristics, especially for bioassay applications such as diagnostic tests.

Introduction

High aspect ratio polymer micropillars have received a lot of research attention recently due to their unique mechanical, optical, and surface properties. They have been utilized as, e.g., biomimicking dry adhesives,¹ airflow sensors,² and superhydrophobic surfaces.³ Within microfluidics, micropillar arrays have been used as capture surfaces for cells⁴ and biomolecules,⁵ in capillary pumping,⁶ for particle sorting,⁷ and for studying cell behavior.^{8–10} At high aspect ratio and high density, micropillar arrays are prone to collapse due to adhesive and capillary forces during liquid or humid operation or during manufacturing schemes involving liquids, such as lithographic processes. Micropillars collapse towards each other when the capillary force is larger than the opposing elastic force exerted by the pillars and the effect is irreversible when adhesive forces that hold the pillars together exceed the elastic forces that pry them apart.¹¹ While capillary micropillar collapse has been used to create novel functional structures,¹² it is generally undesired due to unpredictable materials

properties on the microscale. High aspect ratios and densities of micropillars are desired in applications where high surface area is sought, e.g. for surface chemical interactions or for high capillary pumping pressure. High aspect ratios and high lateral densities of micropillars are desired in applications where, simultaneously, small interpillar distance and high flow throughput are desirable, e.g. for filtration purposes or for high capillary flow.

In previous work, increased aspect ratios have been achieved by strengthening the mechanical properties of the material, e.g. by reinforcing pillars with stiff materials¹³ or using highly cross-linked polymers as the constituting material.¹⁴ However, these approaches still have limits in aspect ratio, and also exclude utilizing low modulus polymer materials, which often are of special interest in microfluidics for use in flexible devices¹⁵ and self-folding structures.¹⁶ Moreover, low modulus polymer materials open up for new chemical groups, not readily available in highly cross-linked materials. Examples of such materials include photocurable PDMS,¹⁷ polyacrylate hydrogels,¹⁸ and the recently introduced Off-Stoichiometry-Thiol-Enes (OSTE),¹⁹ a polymer system that enables excellent surface control due to inherently available functional groups on its surface.

In contrast to current micropillar array designs, we realize capillary collapse resistance through geometrical design by slanting and interlocking the constituting micropillars in truss-like structures. We explore the geometrical limits of capillary collapse for

^a KTH Royal Institute of Technology, Micro and Nanosystems, Osquidas väg 10, 100 44 Stockholm, Sweden, *E-mail: tommyhar@kth.se

[†] Electronic Supplementary Information (ESI) available: [details of any supplementary information available should be included here]. See DOI: 10.1039/b000000x/

[‡] These authors contributed equally to this work

[§] Present address: Department of Mechanical Engineering, Keio University, 3-14-1 Hiyoshi, Kohoku-ku, Yokohama, Japan

traditional straight micropillar arrays and for slanted interlocked micropillars with the same pitch and diameter and manufactured in the same low modulus polymer. We show the increase in surface area and in porous fraction enabled by the new geometry. We call this novel material Synthetic Microfluidic Paper and demonstrate its use as capillary pumps.

Material design

Fig. 1 illustrates the design and manufacturing of Synthetic Microfluidic Paper using slanted interlocked micropillar geometry. The material consists of four sets of interlocked pillars, all sets inclined with an angle $\phi \approx 40^\circ$ with respect to the vertical axis, and the four sets being in azimuthal directions 0° , 90° , 180° , and 270° , thus causing pillars in different sets to interlock. The geometry is further determined by the interpillar pitch (p), the pillar diameter (d), and the vertical height of the structures (h). The number of interlocking points for every pillar depends on the height and interpillar pitch. We chose lithographic manufacturing, instead of 3D-printing or laser writing, because of its scalability towards volume manufacturing and the ease with which sub 100 micron features are replicated. All devices are manufactured in Off-Stoichiometry-Thiol-Ene (OSTE), which previously has demonstrated excellent lithographic properties²⁰ and easy surface modification²¹. To realize the slanted pillar geometry, we utilize multidirectional UV-lithography, previously used for stoichiometric Thiol-Ene²² and Thiol-Ene-Epoxy²³ and which is here realized in a single exposure using an angled mirror setup as illustrated in Fig. 1c (see Fig. S2 in ESI† for photo and details).

Materials and Methods

Manufacturing: The manufacturing process is performed in four steps: (multidirectional) photopatterning, developing, flood curing, and drying. Straight micropillar arrays are formed by vertical illumination through a photomask containing circular openings; slanted interlocked micropillars structures in Synthetic Microfluidic Paper are formed by multidirectional lithography through the same mask. Multidirectional lithography is achieved by reflecting the vertically collimated light to angles of 60° using four aluminum mirrors. OSTE polymer consists of Tetraallyloxyethane (Tokyo Chemical Industry Co., Ltd., Japan) and Tris[2-(3-mercaptopropionyloxy) ethyl] (BOC Sciences, NY, USA) with 40% thiol group excess, and 1% of Irgacure (BASF Corp., USA) and 1% effective weight of Q1301 (Wako Chemical Inc., USA) in saturated toluene (Sigma-Aldrich, USA) solution. Development is done in butyl acetate (VWR, USA).

Capillary collapse testing: The micropillar geometries tested feature pillar diameters of $d = 10\text{--}100\ \mu\text{m}$, pitch $p = 30\text{--}400\ \mu\text{m}$, and height $h = 50\text{--}450\ \mu\text{m}$. The Young's modulus of a fully cured OSTE material slab was measured to be 5.5 MPa using dynamic mechanical and thermal analysis (DMTA) (DMA Q800, PerkinElmer, Waltham, USA). To test the structural resistance against capillary collapse, drying of the butyl acetate developer under a fumehood during the last manufacturing step is used, followed by visualization of the resulting pillar array geometry using microscopy. The contact angle of butyl-acetate, having a surface energy of $0.0251\ \text{Nm}^{-1}$, to OSTE surface was measured

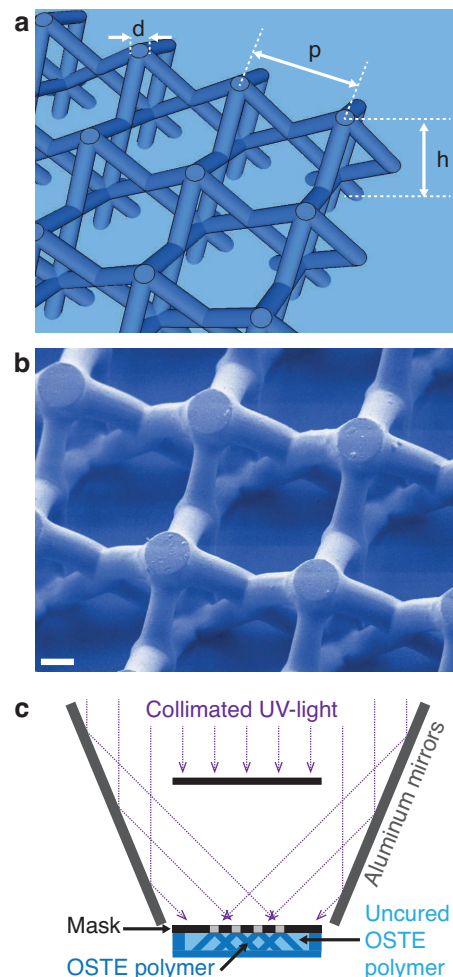


Fig. 1 Geometry and manufacturing of Synthetic Microfluidic Paper, formed by slanted interlocked micropillars. (a) 3D schematic of slanted interlocked micropillar array geometries. (b) Example of a manufactured slanted interlocked micropillars, illustrated by false colored SEM image. Scale bar is $30\ \mu\text{m}$. (c) Manufacturing setup to pattern the OSTE polymer using multidirectional UV-lithography.

as 5.8° by sessile drop method using Attension Theta Lite (Biolin Scientific, Sweden).

Capillary collapse classification: All tested array geometries were inspected with light microscopy using 4-20x long-range objectives (Leica, Germany) from the top, from an angle, and from a teared-off cross-section when necessary. For arrays difficult to classify (mostly for small geometries), inspection in SEM was also conducted. Pillars were defined as collapsed when pillars were stuck on each other or the bottom surface. Pillars were defined as non-collapsed when adherence to each other or to the bottom surface was not observed. For arrays containing both collapsed and non-collapsed parts, the most prevalent feature defined the classification. Examples of this classification can be seen in Fig. 2 c-f. Manufacturing failures defined the classification when $\geq 90\%$ of the array failed. Overcuring, specifically, was detected by polymer structures extending between pillars and blocking the void between interlocked pillars, i.e. in the masked regions.

Solvent uptake in OSTE: The mass of a fully cured OSTE slab,

1 mm x 11 mm x 27 mm, measured with a scale (Kern ABS, Germany), before and after incubation in butyl acetate for 48 h. The drop in mechanical properties in the soaked sample was confirmed by manual manipulation of the sample using tweezers.

Hydrophilic surface treatment: The fabricated OSTE devices prepared for capillary filling experiments was rendered hydrophilic by UV grafting of HEMA. A solution of 5% hydroxyethylmethacrylate (HEMA), 0.1% Lucirin TPO-L (BASF Corp., USA), and 0.1% Benzophenone (BP) (Sigma-Aldrich, USA) in Isopropyl alcohol (IPA) (SunChem AB, Sweden) was prepared. A glass slide was placed above the device, with 150 μm spacing between the top surface of the interlocked pillar array and the glass slide, where the solution was injected. Collimated UV-light was illuminated onto the solution and the pillar array through the glass slide for 300 seconds. After the exposure, the pillar array was rinsed with pure IPA, soaked and incubated with pure IPA for 300 seconds, and dried in room temperature.

Capillary filling: Three types of capillary driven devices ((d , p , h) = (100, 150, 150), (100, 100, 150), and (20, 40, 150) μm) were prepared in 5 mm wide strips and subjected to a hydrophilic surface treatment. For blood imbibition, 30 μl of human blood (sample was collected from healthy human subject, after informed signed consent was obtained) was applied onto one end of a device with a pipette. For water imbibition, the devices were put into contact with a water meniscus defined between 2 glass-slides, 1 mm apart. Filling of the devices was recorded by a camera (EOS 500D, Canon, Japan) and analyzed in Matlab using a threshold algorithm for one image per second of the recorded movie.

Results and Discussion

Capillary collapse resistance

Fig. 2 shows the result from the capillary collapse resistance testing, which is performed by evaporating solvent from interlocked pillar arrays and from straight pillar arrays, each of 150 μm height. Fig. S3 (see ESI†) shows corresponding results for arrays of 50, 300, and 450 μm height. We first discuss the comprehensive results in Fig. 2 and then see that the additional data in Fig. S3 confirms our conclusions.

For straight pillar arrays, indicated by filled circles in Fig. 2a, and imaged in Fig. 2c, collapse resistance is achieved when the pillar diameter, d , and pitch, p , are not too small. Pillars 10 μm in diameter collapse even at high pitch, which can be explained by ground collapse, i.e. the capillary interaction between the pillars and the bottom surface.²⁴ The limit of ground collapse, which is independent of the pitch, can here be estimated between $d = 10$ μm and $d = 20$ μm and is indicated by a red dotted line in Fig. 2a.

The theoretical limit of capillary collapse for straight pillars is plotted as a solid red line in Fig. 2a, based on an approximation of the theory from Chandra and Yang¹¹ for OSTE as constituting material and butyl acetate as liquid medium ($E_{\text{OSTE}} = 5.5$ MPa, contact angle $\theta = 5.8^\circ$, and interfacial energy, $\gamma_{\text{liquid-vapour}} = 0.025$ Nm^{-1} ;²⁵ see ESI† for details). Theory and experimental results are in good agreement for pillar diameters $d \geq 50$ μm , whereas

for smaller pillar diameters, the pillars collapse at a much larger pitch than predicted by theory. We speculate that this might be caused by the influence of the solvent on the mechanical and geometrical properties of the pillars: experiments reveal 8% weight increase and a significant decrease in E-modulus of the pillars when exposed to the solvent. The exact E-modulus of the pillars during evaporation is difficult to measure; however, the effect of the solvent can be expected to be more severe for small pillar diameters due to their increased surface to volume ratio, which would explain the deviation from theory for these geometries. Additionally, the propensity for capillary collapse of small diameter straight pillars emphasizes the need for capillary collapse resistant alternatives.

Non-collapsing slanted interlocked micropillars, indicated by filled squares in Fig. 2b, are achieved for a substantially larger range of pitches and diameters than for straight pillar arrays. Slanted interlocked micropillars only collapse where diameter $d = 10$ μm and pitch $p \geq 60$ μm . Interlocked pillars thus withstand collapse for pitches and diameters below the theoretical limits of straight pillars. Part of the explanation for this can be found in the mechanical nature of the interlocked micropillars. Whereas freely suspended straight pillars collapse by bending¹¹ (seen in Fig. 2c), interlocked pillar collapse by buckling (see Fig. 2f). Moreover, the interlocking points partition each pillar in shorter sections, which are more difficult to deform, and which have a section length,

$$L = \frac{p-d}{2 \sin \theta} \quad (1)$$

that decreases with interpillar pitch and is independent from the overall structure height, h . Collapse occurs when the capillary force, F_c , is larger than the restoring elastic force of the pillar, F_e . The dependence of these forces on the geometrical parameters is

$$F_c \propto \frac{d^2}{p-d} \quad (2)$$

$$F_{e,\text{straight+bending}} \propto \frac{d^4}{h^3} \quad (3)$$

$$F_{e,\text{interlocked+buckling}} \propto \frac{d^4}{(p-d)^2} \quad (4)$$

i.e., with decreasing interpillar distance, $p-d$, the capillary force, F_c , increases linearly; the mechanical strength of straight pillars against bending, $F_{e,\text{straight+bending}}$, remains unaltered; but the critical buckling strength of interlocked pillars, $F_{e,\text{interlocked+buckling}}$, increases quadratically. Consequently, straight pillar arrays collapse with decreasing interpillar distance, whereas slanted interlocked pillar arrays become increasingly more collapse resistant. The current limit in decreasing the interpillar distance is the manufacturing scheme: we observe overcurving, manifested as pillar broadening, which depends on diffraction of light and on the exact UV-exposure time, and which could be optimized in future work.

During capillary collapse testing, an interesting dynamic process was observed while solvent evaporated from the slanted interlocked pillars. Fig. 3 shows how, first, the capillary force causes

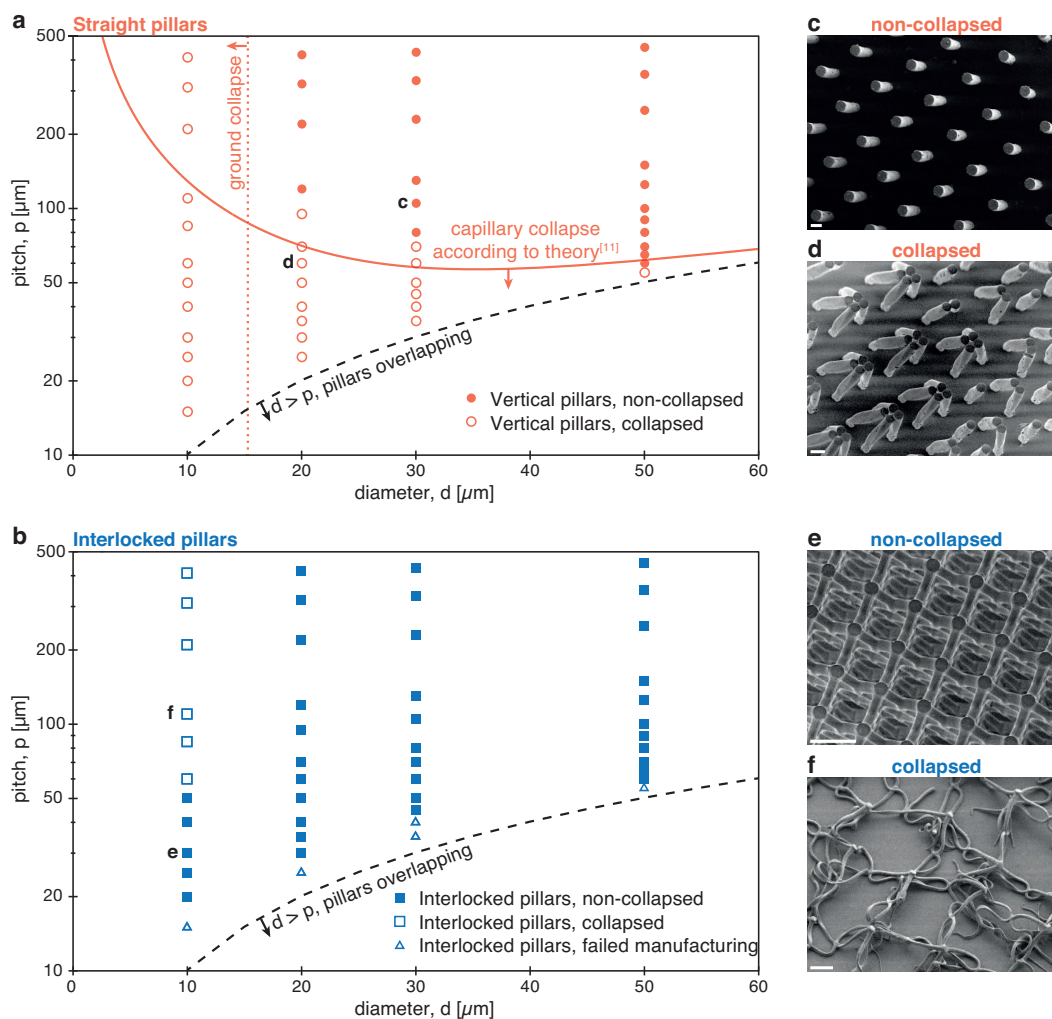


Fig. 2 Capillary collapse resistance of straight micropillar arrays compared to Synthetic Microfluidic Paper (slanted interlocked micropillar arrays). Test structures are of height $h = 150 \mu\text{m}$, fabricated using a photolithography mask with a square pattern of openings with diameter d and pitch p . (a-b) Plots of the results for different opening diameter and pitch for (a) straight pillars and (b) slanted interlocked pillars. The diameters of pillars tested are 10, 20, 30, and $50 \mu\text{m}$. The solid red line in (a) indicates the theoretical capillary collapse limit for straight pillars; the dotted red line in (a) indicated the limit of ground collapse observed, and the dashed black line in (a) and (b) indicates where pillars overlap ($p > d$). (c-f) SEM images of (c) a non-collapsed straight pillar array at $d = 30 \mu\text{m}$, $p = 105 \mu\text{m}$, and $h = 150 \mu\text{m}$, (d) a collapsed straight pillar array at $d = 20 \mu\text{m}$, $p = 60 \mu\text{m}$, and $h = 150 \mu\text{m}$, (e) a non-collapsed slanted interlocked micropillar array at $d = 10 \mu\text{m}$, $p = 30 \mu\text{m}$, and $h = 150 \mu\text{m}$, and (f) a collapsed slanted interlocked micropillar array at $d = 10 \mu\text{m}$, $p = 110 \mu\text{m}$, and $h = 150 \mu\text{m}$. Scale bars are $30 \mu\text{m}$.

part of the slanted interlocked micropillars to collapse down towards the substrate. While the solvent evaporated, the energy stored in the buckled pillars restored the structure to its original non-collapsed geometry. This phenomenon was observed for a few structures with relatively large pitch and small diameter ($d = 20 \mu\text{m}$ and $p = 100 \mu\text{m}$, for $h = 150$ and 300), but not for larger diameters and smaller pitches. This self-restoring property only applies to elastomeric or low modulus materials, and could potentially be utilized in self-folding micro- or macrostructures in future developments.

Increased surface area and porous fraction

Due to their capillary collapse resistance, the slanted interlocked micropillar arrays of Synthetic Microfluidic Paper provide two specific benefits over straight pillar arrays: increased surface area

and increased porous fraction.

The increase in solid surface area A_p compared to the device footprint area, A_{fp} ,

$$\eta = \frac{A_p}{A_{fp}} \quad (5)$$

is a measure for the potential of the device for surface capturing assays, such as cell or biomolecular capturing. Fig. 4a illustrates that the area increase scales inversely with pillar diameter and pillar pitch. The maximum increase for straight pillars is 7.5, whereas the best area increase for slanted interlocked pillars is 45, i.e. a six-fold increase. This is a direct result of the capillary collapse resistance, which allows thinner and denser pillar arrays. Moreover, each p^2 unit of footprint area contains one straight pillar, but four slanted interlocked pillars. The porous fraction for lateral flow, f_p , is the pore area (i.e. the interpillar area) per total

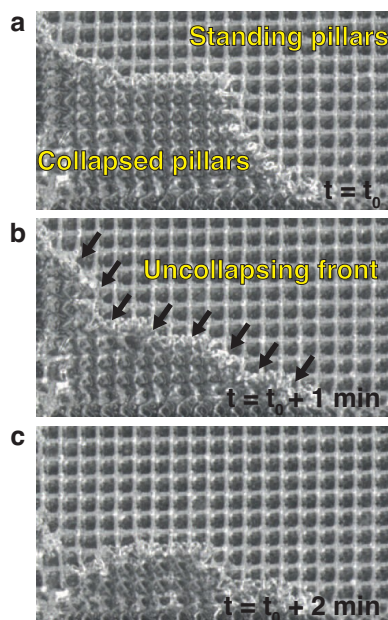


Fig. 3 Top view microscopic images of slanted interlocked pillars with $d = 20 \mu\text{m}$ and $p = 100 \mu\text{m}$ during drying, taken with one minute intervals.

area, i.e.

$$F_{fp} = \frac{p-d}{p} \quad (6)$$

Fig. 4b shows the relative increase of the porous fraction of slanted interlocked pillars compared to straight pillars for different values of the interpillar distance $p-d$. The relative porous fraction of slanted interlocked pillars increases with decreasing interpillar distance, and is three times larger for $10 \mu\text{m}$ interpillar distance arrays. This increase is the result of the interlocking design, which allows for a smaller pillar diameter at a given interpillar distance. The relative increase in porous fraction for Synthetic Microfluidic Paper is expected to allow for an equal increase in flow throughput in capillary pumping and particle sorting or filtering applications, for the same capillary pressure and filter cut-off values, respectively.

Capillary pumping

To demonstrate its practical use in microfluidic applications, 5 mm wide strips of Synthetic Microfluidic Paper, consisting of capillary pumps. Geometries of the hydrophilic slanted interlocked micropillar arrays were chosen to demonstrate pumped volume and flow rates relevant for lateral flow assays, i.e. similar as previous lateral flow assay materials. First, the free surface thiol groups of the OSTE polymer are utilized to bind hydrophilic HEMA molecules, resulting in a lowered surface contact angle of 25° for DI-water. A drop of human blood is placed on top of the strip, resulting in imbibition of the blood into the Synthetic Microfluidic Paper. Fig. 5a-b shows the capillary flow of blood in Synthetic Microfluidic Paper with geometries ($d = 50 \mu\text{m}$, $p = 150 \mu\text{m}$, $h = 150 \mu\text{m}$), ($d = 50 \mu\text{m}$, $p = 100 \mu\text{m}$, $h = 150 \mu\text{m}$), and ($d = 20 \mu\text{m}$, $p = 40 \mu\text{m}$, $h = 150 \mu\text{m}$), demonstrat-

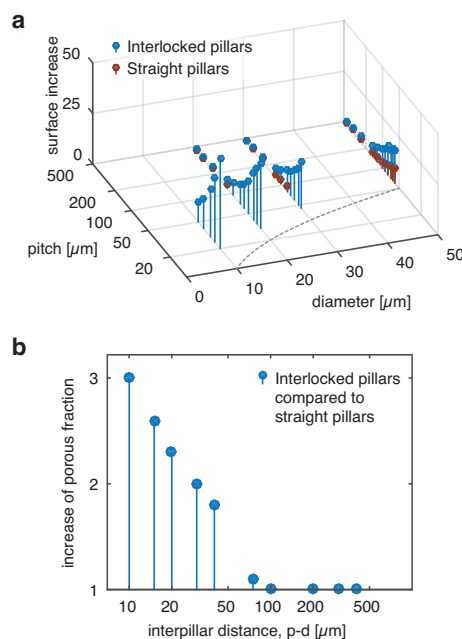


Fig. 4 Geometrical improvements of straight micropillar arrays compared to Synthetic Microfluidic Paper of height $h = 150 \mu\text{m}$. (a) Surface increase of non-collapsed interlocked pillars and straight pillars compared to a flat surface. The maximum surface increase is 45 fold for interlocked pillars and 7.5 fold for straight pillars, hence interlocked pillars provide a 6 fold improvement over straight pillars. The grey dashed line indicates $p=d$. (b) The maximum porous fraction for lateral flow of non-collapsed interlocked pillars, normalized to the maximum porous fraction of non-collapsed straight pillars for the same interpillar distance. The porous fraction scales linearly with the filtration capacity of the device when used as filter, and with the flow capacity of the device when used as capillary pump.

ing volumetric pumping capacities of $16 \mu\text{l}$, $6 \mu\text{l}$, and $9 \mu\text{l}$ in one minute, respectively. Least mean square regression fitting shows that the blood liquid front propagation scales approximately ($R^2 = 0.99, 0.98,$ and $0.97,$ respectively) with $t^{1/2}$, as expected from the Washburn equation, with liquid front velocities of $1.7 \text{ mm s}^{-1/2}$, $1.8 \text{ mm s}^{-1/2}$, and $2.0 \text{ mm s}^{-1/2}$, respectively. This flow behavior indicates that the material is suitable as a capillary pump, and that the pumping rate makes it a potential alternative to other porous microfluidic materials, such as paper, nitrocellulose or straight micropillar arrays. Comparable flowrates in other materials have been reported previously, e.g. $4 \text{ mm s}^{-1/2}$ in a polymer micropillar array⁶ for serum (serum having 2-3 times lower viscosity than blood) and $1.6 \text{ mm s}^{-1/2}$ for blood in nitrocellulose.²⁶ The slight deviations from the Washburn equation follow mainly from our experimental measurement setup and the difficulty of exactly determining the starting point of propagation from an imprecisely placed blood drop.

Fig. 5c shows water imbibition tests from a well-defined water meniscus, on 4 devices Synthetic Microfluidic Paper with identical geometries ($d = 50 \mu\text{m}$, $p = 150 \mu\text{m}$, $h = 150 \mu\text{m}$), resulting in a liquid flow speed $9.9 \text{ mm s}^{-1/2}$, i.e. 4 cm in 16 s, with a standard deviation of 2%. This is a considerable improvement over commercial nitrocellulose substrates, which features a liquid pumping speed of 75 s for 4 cm for the fastest nitrocellulose substrate, with

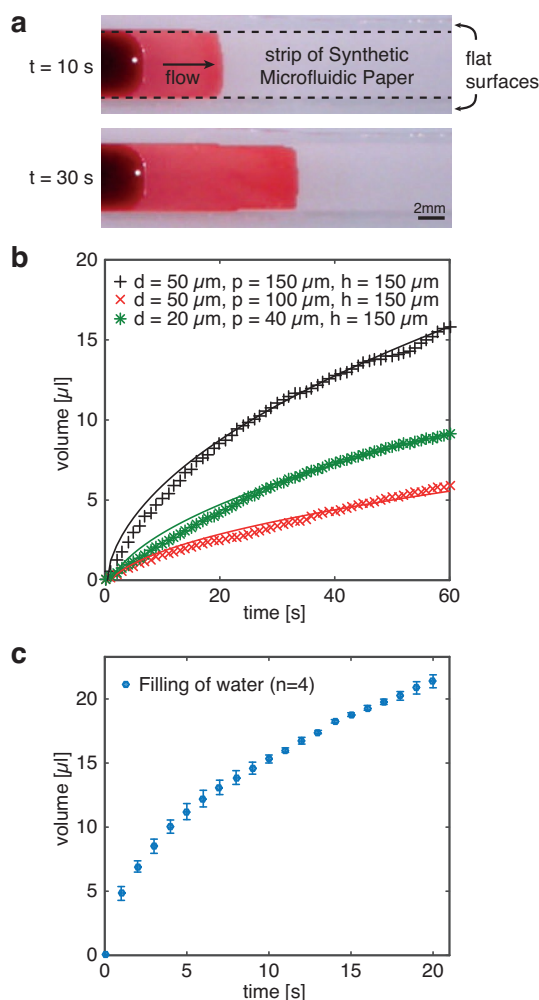


Fig. 5 Capillary filling in Synthetic Microfluidic Paper (a) Photos of a strip of a Synthetic Microfluidic Paper during capillary filling of whole blood for $d = 50 \mu\text{m}$, $p = 150 \mu\text{m}$, $h = 150 \mu\text{m}$ after 10 and 30 s of filling. (b) Measured capillary filling of blood in the Synthetic Microfluidic Paper, and their least mean square regression fitting, assuming Washburn behaviour (solid lines). (c) Measured capillary filling and standard deviation of water in Synthetic Microfluidic Paper with geometries $d = 50 \mu\text{m}$, $p = 150 \mu\text{m}$, $h = 150 \mu\text{m}$.

a standard deviation of 8%.²⁷

Other potential applications

The successful covalent surface modification of the slanted interlocked micropillars indicates the versatility of the material and motivates other future potential microfluidic applications, such as high area/volume biosensing surfaces.

Although not experimentally tested, we can speculate on the use of slanted interlocked pillars for other applications. The surface area increase makes our novel geometry especially beneficial for microfluidic applications relying on high capture surface^{4,5}. The combination of controlled surface properties, capillary evaporation, and the possibility to use low E-modulus polymers provides new possibilities for flexible devices and bioinspired self-folding materials. Our slanted interlocked pillars may be suitable for use as biomimicking dry adhesives, which rely on sub-

micrometer pillar features, with an as high as possible number of pillars capable of attaching to a surface ($\sim p^{-2}$), and which particular geometry (h, d) is of less importance, as long as pillars are flexible enough to attach to uneven surfaces without break, curl or tangle.¹ The slanted pillar design introduced here may allow increasing the pillar density, although this would require further development of the 3D manufacturing to the sub-micrometer scale. The structure is indeed superhydrophobic³ for its native surface, but airflow sensing,² relying on flexible pillars, can be expected to have an inverse effect on sensitivity at low flowrates. For particle sorting applications, the increased porous fraction is beneficial. Moreover, the 3D nature of this material could open up particle sorting in two dimensions instead of only one, as for straight pillars.⁷

Conclusions

We introduce Synthetic Microfluidic Paper, consisting of slanted interlocked micropillar arrays, as a novel porous substrate material in microfluidics. We studied this novel microfluidic material as an alternative to traditional straight micropillar arrays and to nitrocellulose. We show that, compared to straight micropillar arrays, Synthetic Microfluidic Paper features higher resistance to capillary collapse, even beyond the fundamental limitations of capillary collapse for straight micropillar arrays. This results in a material with up to six-fold increased surface area and up to three times higher porous fraction compared to straight micropillar arrays. The latter is expected to allow increase in flow throughput in capillary pumping and particle sorting or filtering applications. We also demonstrate the use of Synthetic Microfluidic Paper for reliable capillary pumps. Compared to nitrocellulose, Synthetic Microfluidic Paper shows a wider range of pumping speeds and four times lower device-to-device variation. We foresee future applications of the material, e.g. in biosensing applications and self-folding structures.

Acknowledgements

This work has been sponsored in part by the European Commission through the FP7 project ROUTINE. We thank Linnea Gustavsson for help with SEM imaging.

References

- 1 A. K. Geim, S. V. Dubonos, I. V. Grigorieva, K. S. Novoselov, A. A. Zhukov and S. Y. Shapoval, *Nature Materials*, 2003, **2**, 461–463.
- 2 J. Paek and J. Kim, *Nature Communications*, 2014, **5**, year.
- 3 X.-M. Li, D. Reinhoudt and M. Crego-Calama, *Chemical Society Reviews*, 2007, **36**, 1350–1368.
- 4 S. Nagrath, L. V. Sequist, S. Maheswaran, D. W. Bell, D. Irimia, L. Ulkus, M. R. Smith, E. L. Kwak, S. Digumarthy, A. Muzikansky, P. Ryan, U. J. Balis, R. G. Tompkins, D. A. Haber and M. Toner, *Nature*, 2007, **450**, 1235–1239.
- 5 M. M. Dudek, T. L. Lindahl and A. J. Killard, *Analytical Chemistry*, 2010, **82**, 2029–2035.
- 6 C. Jönsson, M. Aronsson, G. Rundström, C. Pettersson, I. Mendel-Hartvig, J. Bakker, E. Martinsson, B. Liedberg,

- B. MacCraith, O. Öhman and J. Melin, *Lab on a Chip*, 2008, **8**, 1191–1197.
- 7 J. McGrath, M. Jimenez and H. Bridle, *Lab on a Chip*, 2014, **14**, 4139–4158.
- 8 I. Y. Wong, S. Javaid, E. A. Wong, S. Perk, D. A. Haber, M. Toner and D. Irimia, *Nature Materials*, 2014, **13**, 1063–1071.
- 9 L. Trichet, J. L. Digabel, R. J. Hawkins, S. R. K. Vedula, M. Gupta, C. Ribault, P. Hersen, R. Voituriez and B. Ladoux, *Proceedings of the National Academy of Sciences*, 2012, **109**, 6933–6938.
- 10 L. Aoun, P. Weiss, A. Laborde, B. Ducommun, V. Lobjois and C. Vieu, *Lab on a Chip*, 2014, **14**, 2344–2353.
- 11 D. Chandra and S. Yang, *Langmuir*, 2009, **25**, 10430–10434.
- 12 B. Pokroy, S. H. Kang, L. Mahadevan and J. Aizenberg, *Science*, 2009, **323**, 237–240.
- 13 H. Yoon, M. K. Kwak, S. M. Kim, S. H. Sung, J. Lim, H. S. Suh, K. Y. Suh and K. Char, *Small*, 2011, **7**, 3005–3010.
- 14 J. D. Williams and W. Wang, *Journal of Micro/Nanolithography, MEMS, and MOEMS*, 2004, **3**, 563–568.
- 15 C. Liao, M. Zhang, M. Y. Yao, T. Hua, L. Li and F. Yan, *Advanced Materials*, 2014, n/a–n/a.
- 16 L. Ionov, *Polymer Reviews*, 2013, **53**, 92–107.
- 17 W. Chen, R. H. W. Lam and J. Fu, *Lab on a Chip*, 2011, **12**, 391–395.
- 18 A. Revzin, R. J. Russell, V. K. Yadavalli, W.-G. Koh, C. Deister, D. D. Hile, M. B. Mellott and M. V. Pishko, *Langmuir*, 2001, **17**, 5440–5447.
- 19 C. F. Carlborg, T. Haraldsson, K. Öberg, M. Malkoch and W. van der Wijngaart, *Lab on a Chip*, 2011, **11**, 3136.
- 20 G. Pardon, F. Saharil, J. M. Karlsson, O. Supekar, C. F. Carlborg, W. van der Wijngaart and T. Haraldsson, *Microfluidics and Nanofluidics*, 2014, 1–7.
- 21 F. Carlborg, F. Moraga, F. Saharil, W. van der Wijngaart and T. Haraldsson, The 16th International Conference on Miniaturized Systems for Chemistry and Life Sciences, Okinawa, Japan, Oct 28 - Nov 1, 2012, pp. 677–679.
- 22 A. J. Jacobsen, W. Barvosa-Carter and S. Nutt, *Advanced Materials*, 2007, **19**, 3892–3896.
- 23 J. Hansson, H. Yasuga, T. Haraldsson and W. van der Wijngaart, 2015 28th IEEE International Conference on Micro Electro Mechanical Systems (MEMS), 2015, pp. 10–13.
- 24 P. Roca-Cusachs, F. Rico, E. Martínez, J. Toset, R. Farré and D. Navajas, *Langmuir*, 2005, **21**, 5542–5548.
- 25 J. A. Riddick, W. B. Bunger and T. K. Sakano, *Organic Solvents: Physical Properties and Methods of Purification*, Wiley-Interscience, New York, 4th edn, 1986.
- 26 H. Li, D. Han, G. M. Pauletti and A. J. Steckl, *Lab on a Chip*, 2014, **14**, 4035–4041.
- 27 Millipore, *Hi-Flow™ Plus Membranes and SureWick® Pad Materials*, 2013.